

## N<sub>2</sub> Fixation

# CO-Induced Dinitrogen Fixation and Cleavage Mediated by Boron

Guohai Deng<sup>+, [a]</sup> Sudip Pan<sup>+, [b, c]</sup> Xuelin Dong,<sup>[a]</sup> Guanjun Wang,<sup>[a]</sup> Lili Zhao,<sup>[b]</sup> Mingfei Zhou,<sup>\*, [a]</sup> and Gernot Frenking<sup>\*, [b, c]</sup>

**Abstract:** The boron atoms react with carbon monoxide and dinitrogen forming the end-on bonded NNBCO complex in solid neon or in nitrogen matrices. The NNBCO complex rearranges to the ( $\eta^2$ -N<sub>2</sub>)BCO isomer with a more activated side-on bonded dinitrogen ligand upon visible light excitation. ( $\eta^2$ -N<sub>2</sub>)BCO and its weakly CO-coordinated complexes

further isomerize to the NBNCO and B(NCO)<sub>2</sub> molecules with N–N bond being completely cleaved under UV light irradiation. The geometries, energies and vibrational spectra of the molecules are calculated with quantum chemical methods and the electronic structures are analyzed with charge- and energy-partitioning methods.

## Introduction

Although dinitrogen is an abundant and easily accessible resource, its utilization is one of the long-standing important and challenging topics in chemistry, due to the extremely inertness of the N≡N triple bond.<sup>[1]</sup> Both the natural nitrogenase enzymes and the industrial Haber–Bosch ammonia synthesis processes rely on transition metal centers to catalyze the dinitrogen fixation and transformation reactions.<sup>[2,3]</sup> The unique ability of these transition metal compounds to bind and activate N<sub>2</sub> is attributed to the partially filled d orbitals of the metal, which can synergically accept electron density from filled  $\sigma$  orbitals of N<sub>2</sub> (termed as  $\sigma$  donation) and backdonate  $d_{\pi}$  electrons to the antibonding  $\pi^*$  orbitals of N<sub>2</sub> ( $\pi$  backdonation).<sup>[4–7]</sup> Due to the lack of accessible d orbitals, main group elements are expected to have very limited ability to bind and

activate N<sub>2</sub>. However, recent reports demonstrated that the borylene complexes featuring reactive lone pairs of electrons as well as vacant orbitals at the monovalent boron atom effectively mimic transition metals that can fix and reduce N<sub>2</sub>.<sup>[8]</sup> This provides a new pathway for nitrogen reduction reaction by a nonmetal main group element at ambient conditions.<sup>[8–10]</sup>


Main group atoms with (ns)<sup>2</sup>(np)<sup>x</sup> (x = 0–6) ground state electronic configurations are generally not bound to N<sub>2</sub>. Only very few dinitrogen complexes of main group elements have been reported with limited level of N<sub>2</sub> activation due to the lack of strong  $\pi$  back donation.<sup>[11–17]</sup> Thus, the dinitrogen ligands can hardly be further activated or functionalized. CO is isoelectronic with N<sub>2</sub> and serves as a better ligand than N<sub>2</sub> for donor–acceptor bonding with metal centers. It has been shown that dinitrogen coordination and cleavage can be effectively induced by CO with concomitant N–C bond formation mediated by transition metal complexes.<sup>[18–20]</sup> CO-induced dinitrogen fixation and activation can serve as an alternative route for dinitrogen transformations.<sup>[18–21]</sup> It has been found that many main group atoms can readily react with carbon monoxide in forming various carbonyl complexes.<sup>[22–30]</sup> This opens the possibility of dinitrogen coordination and activation via coupling with carbon monoxide mediated by main group elements. Our recent studies on the reactions of beryllium atoms with carbon monoxide and dinitrogen mixtures have already demonstrated that dinitrogen coordination and activation can be achieved by beryllium via coupling with carbon monoxide.<sup>[31]</sup> Here, we report a joint matrix-isolation infrared-spectroscopic and theoretical study on dinitrogen fixation and cleavage via coupling with carbon monoxide mediated by boron atoms in forming isocyanate complexes NBNCO and B(NCO)<sub>2</sub> with the N–N triple bond being completely cleaved. The results show that the N≡N activation processes proceed with the initial formation of an end-on bonded NNBCO complex, which rearranges to the NBNCO and B(NCO)<sub>2</sub> isocyanate complexes via a side-on bonded ( $\eta^2$ -N<sub>2</sub>)BCO intermediate.


[a] G. Deng,<sup>+</sup> X. Dong, Prof. Dr. G. Wang, Prof. Dr. M. Zhou  
 Collaborative Innovation Center of Chemistry for Energy Materials  
 Department of Chemistry, Shanghai Key Laboratory of  
 Molecular Catalysts and Innovative Materials, Fudan University  
 Shanghai 200438 (China)  
 E-mail: mfzhou@fudan.edu.cn

[b] Dr. S. Pan,<sup>+</sup> Prof. Dr. L. Zhao, Prof. G. Frenking  
 Institute of Advanced Synthesis, School of Chemistry and  
 Molecular Engineering, Jiangsu National Synergetic Innovation Center for  
 Advanced Materials, Nanjing Tech University, Nanjing 211816 (China)

[c] Dr. S. Pan,<sup>+</sup> Prof. G. Frenking  
 Fachbereich Chemie, Philipps-Universität Marburg  
 Hans-Meerwein-Strasse 4, 35043 Marburg (Germany)  
 E-mail: frenking@chemie.uni-marburg.de

[<sup>+</sup>] These authors contributed equally to this work.

 Supporting information and the ORCID identification number(s) for the author(s) of this article can be found under:  
<https://doi.org/10.1002/chem.202004357>.

 © 2020 The Authors. Chemistry - A European Journal published by Wiley-VCH GmbH. This is an open access article under the terms of the Creative Commons Attribution Non-Commercial NoDerivs License, which permits use and distribution in any medium, provided the original work is properly cited, the use is non-commercial and no modifications or adaptations are made.

## Results and Discussion

### Experimental Results

#### Infrared spectra

The infrared spectra in the 2360–1860  $\text{cm}^{-1}$  frequency region using a  $^{10}\text{B}$ -enriched boron target and 0.03%  $\text{CO} + 0.3\%$   $\text{N}_2$  mixture sample in neon are illustrated in Figure 1. After 30 min of sample deposition at 4 K, boron carbonyl stretching vibrations are observed. The bands at 2014.2/2012.0  $\text{cm}^{-1}$  are attributed to the C–O stretching vibration of the  $^{10}\text{BCO}$  molecule at two trapping sites.<sup>[25,32]</sup> The 2031.1  $\text{cm}^{-1}$  band corresponds to the band reported at 2022.5  $\text{cm}^{-1}$  in solid argon that was previously assigned to the antisymmetric C–O stretching vibration of the linear  $^{10}\text{B}(\text{CO})_2$  molecule. Besides the boron carbonyl absorptions, new product absorptions are observed either on sample deposition or on annealing or photolysis. These absorptions are only produced in the experiments when both the  $\text{N}_2$  and  $\text{CO}$  samples are employed, and can be classified into several groups based on their annealing and photochemical behaviors (labeled as A–E in Figure 1). Species involve more than one boron atoms, such as  $\text{BBCO}$ ,  $\text{OCBBCO}$ ,  $\text{B}_4(\text{CO})_2$ <sup>[26]</sup> and  $\text{BBNN}$ ,<sup>[33]</sup> which were reported previously to be the major products from the reactions of laser-ablated boron atoms with  $\text{CO}$  or  $\text{N}_2$  in solid argon or nitrogen matrices are barely observed with relatively low ablation laser energy used in the present experiments.

Species A has two bands at 2041.4 and 1900.5  $\text{cm}^{-1}$ , both are observed on sample deposition and markedly increase on sample annealing to 12 K, but decrease under visible (435–480 nm) and UV-visible ( $250 < \lambda < 580$  nm) light irradiation. The group A absorptions are the dominated absorptions observed at the experimental conditions employed for Figure 1. Three

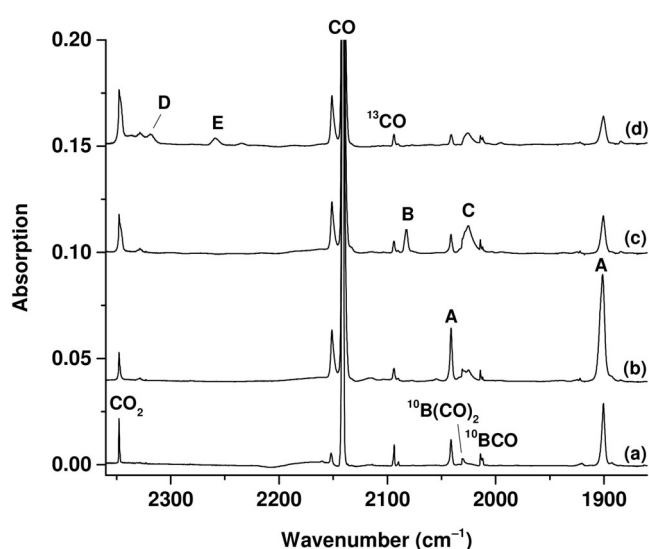


**Figure 1.** Infrared spectra in the 2360–1860  $\text{cm}^{-1}$  region from co-deposition of laser ablated  $^{10}\text{B}$ -enriched boron atoms with 0.03%  $\text{CO} + 0.3\%$   $\text{N}_2$  in neon. (a) after 30 min of sample deposition at 4 K; (b) after annealing to 12 K; (c) after 30 min of visible light irradiation; and (d) after 15 min of UV light irradiation. A:  $\text{NNBCO}$ ; B:  $(\eta^2\text{-N}_2)\text{BCO}$ ; C:  $\text{N}_2\text{-B}(\text{CO})_2$ ; D:  $\text{NBNCO}$ ; E:  $\text{B}(\text{NCO})_2$ .

bands at 2083.1, 1600.2 and 1182.8  $\text{cm}^{-1}$  are observed for species B with comparable IR intensities. The two low frequency modes are not shown in Figure 1 (see Figures S1 and S2). These absorptions are produced only under visible light (435–480 nm) irradiation when the group A absorptions decrease. The group B absorptions are completely destroyed upon irradiation with UV light ( $250 < \lambda < 580$  nm). Only one broad band centered at 2025  $\text{cm}^{-1}$  is observed for species C. It increases both on sample annealing and visible light irradiation, but markedly decreases upon UV light irradiation. This band is only about 5  $\text{cm}^{-1}$  red-shifted from the antisymmetric CO stretching mode of the linear  $\text{B}(\text{CO})_2$  molecule and can be attributed to the weakly bound  $\text{N}_2\text{-B}(\text{CO})_2$  complex. Both species D and E are produced only under UV light irradiation and only one band is observed for each species.

A series of experiments are performed using different concentrations of  $\text{CO}$  and  $\text{N}_2$  in excess neon. The spectra in the same region as Figure 1 from an experiment using a 0.1%  $\text{CO} + 0.1\%$   $\text{N}_2$  sample are shown in Figure S3. With the relative concentration of  $\text{CO}$  increases, the yields of the boron carbonyl species  $\text{BCO}$ ,  $\text{B}(\text{CO})_2$  as well as the  $\text{N}_2\text{-B}(\text{CO})_2$  (C) complex increase. The yield of species E also increases with respect to species D. The bands of both species A and B become broader with the band positions slightly blue- or red-shifted when the  $\text{CO}$  concentration increases, suggesting the formation of weakly bound complexes. Additional experiments are also done using dinitrogen as matrix. The spectra from an experiment using  $^{10}\text{B}$ -enriched target and 0.5%  $\text{CO}$  in dinitrogen are shown in Figure 2.

The observed chemistry is quite similar to those in Ne matrix. Sharp band at 2017.8  $\text{cm}^{-1}$  is attributed to  $\text{B}(\text{CO})_2$ . The  $\text{BCO}$  and species C absorptions are absent in the spectra. The two modes of species A are observed at 2041.9 and 1897.1  $\text{cm}^{-1}$ , while species B is observed at 2078.1, 1597.1 and 1181.2  $\text{cm}^{-1}$ . Species E is barely observed, and only species D (2315.5  $\text{cm}^{-1}$ ) is produced upon UV light irradiation in dinitrogen matrix. The band positions of these product species all are slightly red-shifted from those in Ne matrix. Similar experiments are performed using the isotopic-labeled samples including  $^{15}\text{N}_2$ ,  $^{13}\text{CO}$  and  $\text{C}^{18}\text{O}$ , as well as natural abundance boron target. The spectra in selected regions using different isotopic-labeled samples and mixtures are shown in Figures S1, S2 and S4–S8, respectively. The band positions are listed in Table 1.

#### Spectral assignments

Species A with two absorptions at 2041.4 and 1900.5  $\text{cm}^{-1}$  in Ne and at 2041.9 and 1897.1  $\text{cm}^{-1}$  in  $\text{N}_2$  is assigned to the  $\text{NN}^{10}\text{BCO}$  complex. The spectra using different isotopic-labeled samples (Figures S4 and S7) clearly demonstrate that species A involves one boron atom, one  $\text{CO}$  ligand and one  $\text{N}_2$  ligand with two inequivalent N atoms. This complex has been observed in solid argon matrix with the low mode observed at 1892.2  $\text{cm}^{-1}$ .<sup>[34]</sup> The low frequency mode shows quite large nitrogen isotopic shift and is largely a N–N stretching vibration, while the upper mode is mainly C–O vibration. The two

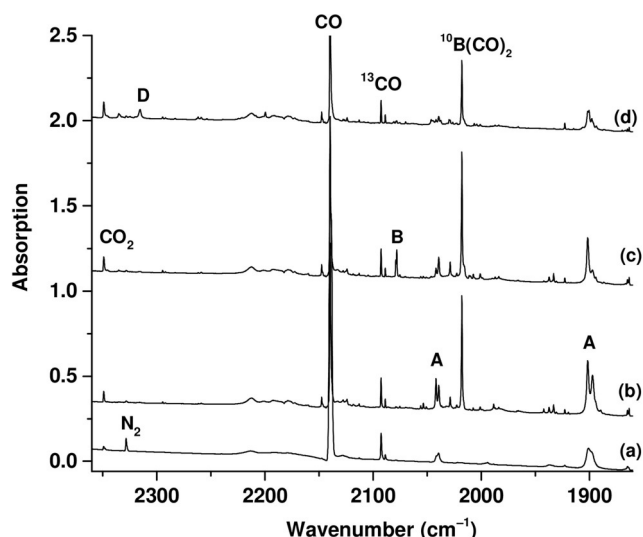


**Figure 2.** Infrared spectra in the 2360–1860  $\text{cm}^{-1}$  region from co-deposition of laser ablated boron ( $^{10}\text{B}$ -enriched) atoms with 0.5% CO in solid nitrogen. (a) after 30 min of sample deposition at 4 K, (b) after annealing to 25 K, (c) after 30 min visible light irradiation, and (d) after 15 min of UV-visible light ( $250 < \lambda < 580 \text{ nm}$ ) irradiation. A: NNBCO; B:  $(\eta^2\text{-N}_2)\text{BCO}$ ; D: NBNCO.

modes are strongly coupled. The upper mode for the  $\text{NN}^{10}\text{B}^{13}\text{CO}$  isotopomer is absent (Figure S4, spectrum c), suggesting that the upper mode can be regarded as the symmetric stretching mode of the nearly symmetric  $\text{NN}^{10}\text{B}^{13}\text{CO}$  isotopomer. Also note that the low mode of the  $^{15}\text{N}^{15}\text{N}^{10}\text{BCO}$  isotopomer splits into two bands at 1853.5 and 1830.6  $\text{cm}^{-1}$  (Figure S4, spectrum f), suggesting the involvement of Fermi resonance. As has been discussed,<sup>[34]</sup> a Fermi resonance of  $\nu_2$  (predicted at 1982.3  $\text{cm}^{-1}$ ) with a combinational mode of  $\nu_3$  (predicted at 1463.8  $\text{cm}^{-1}$ ) and  $\nu_8$  (predicted at 521.2  $\text{cm}^{-1}$ ) can likely take place in this isotopomer.

The group B absorptions are assigned to different vibrational modes of the  $(\eta^2\text{-N}_2)\text{BCO}$  complex. The experiments using different isotopic-labeled mixture samples (Figures S1, S2, and S4) confirm that species B also involves one boron atom, one CO ligand and one  $\text{N}_2$  ligand. The band at 2083.1  $\text{cm}^{-1}$  in Ne shows quite small  $^{15}\text{N}$  and  $^{11}\text{B}$  isotopic shifts but quite large  $^{13}\text{C}$  and  $^{18}\text{O}$  isotopic shifts (Table 1). The band position and isotopic shifts imply that it is a terminal C–O stretching vibration. The band at 1600.2  $\text{cm}^{-1}$  in Ne is largely a N–N stretching mode. The band position and isotopic splittings in the mixed  $\text{N}_2 + ^{15}\text{N}_2/\text{CO}$  and  $\text{N}_2 + ^{14}\text{N}^{15}\text{N} + ^{15}\text{N}_2/\text{CO}$  experiments (Figure S1) confirm that a side-on bonded  $\text{N}_2$  ligand with equivalent nitrogen atoms is involved. The low frequency band at 1182.6  $\text{cm}^{-1}$  in Ne and at 1181.2  $\text{cm}^{-1}$  in  $\text{N}_2$  is attributed to the OC–B– $\text{N}_2$  stretching mode.

The band position and isotopic shifts (Table 1) for species D at 2317.4  $\text{cm}^{-1}$  in neon and 2315.5  $\text{cm}^{-1}$  in  $\text{N}_2$  indicate that this species is an isocyanate complex. The isotopic structures observed in the mixed  $^{12}\text{CO} + ^{13}\text{CO}/\text{N}_2$  and  $\text{C}^{16}\text{O} + \text{C}^{18}\text{O}/\text{N}_2$  experiments (Figure S6) show that only one NCO subunit is involved. The photochemical behavior implies that species D is a structural isomer of species A and B, and thus is assigned to NBNCO. The band position is slightly higher than that of NBeNCO at 2287.5  $\text{cm}^{-1}$  in Ne.<sup>[31]</sup> The same modes of  $\text{Cl}_2\text{BNCO}$ ,  $(\text{CH}_3)_2\text{BNCO}$  and  $\text{F}_2\text{BNCO}$  were reported at 2270, 2285 and 2333  $\text{cm}^{-1}$ , respectively.<sup>[35]</sup> Species E is only observed in solid neon matrix with an absorption at 2259.7  $\text{cm}^{-1}$ . The isotopic shifts indicate that this is also an antisymmetric NCO stretching vibration. The experiments using different isotopic-labeled mixture samples (Figure S5) confirm that two equivalent NCO subunits are involved. Accordingly, species E is assigned to  $\text{B}(\text{NCO})_2$ , a di-isocyanate species.

**Table 1.** Experimental vibrational frequencies ( $\text{cm}^{-1}$ ) of the product species observed in solid neon and dinitrogen (in parentheses) matrices and computed frequencies at the CCSD(T)-Full/cc-pVTZ level.

Molecule	$^{10}\text{B}/\text{CO}/\text{N}_2$	$^{10}\text{B}/\text{CO}/^{15}\text{N}_2$	$\Delta\nu^{[a]}$	$^{10}\text{B}/^{13}\text{CO}/\text{N}_2$	$\Delta\nu^{[a]}$	$^{10}\text{B}/\text{C}^{18}\text{O}/\text{N}_2$	$\Delta\nu^{[a]}$	$^{11}\text{B}/\text{CO}/\text{N}_2$	$\Delta\nu^{[a]}$
Experimental									
NNBCO (A)	2041.4 (2041.9)	2030.0	−11.4	— <sup>[b]</sup>	—	2017.8	−23.6	2035.1	−6.3
$(\eta^2\text{-N}_2)\text{BCO}$ (B)	1900.5 (1897.1)	1853.5	−47.0	1890.9	−9.6	1894.5	−6.0	1892.7	−7.8
	2083.1 (2078.1)	2082.8	−0.4	2034.7	−48.4	2053.8	−29.3	2074.7	−8.4
	1600.2 (1597.1)	1569.8	−30.4	1599.4	−0.8	1593.2	−7.0	1579.9	−20.3
NBNCO (D)	1182.8 (1181.2)	1164.9	−17.9	1181.0	−1.8	1177.0	−5.8	1156.5	−26.3
	2317.4 (2315.5)	2310.5	−16.2	2259.3	−58.1	2300.8	−16.6	2317.3	−0.1
$\text{B}(\text{NCO})_2$ (E)	2259.7	2249.2	−10.5	2199.2	−60.5	2242.2	−17.5	2258.8	−0.9
Computed									
NNBCO (A)	2118.3	2108.4	−9.9	2077.7	−40.6	2092.5	−25.8	2115.7 [154] <sup>[c]</sup>	−2.6
	1988.0	1931.4	−56.6	1975.2	−12.8	1982.3	−5.7	1982.3 [2563] <sup>[c]</sup>	−5.7
$(\eta^2\text{-N}_2)\text{BCO}$ (B)	2150.3	2149.0	−1.3	2097.4	−52.9	2119.7	−30.6	2142.2 [626] <sup>[c]</sup>	−8.1
	1657.4	1625.8	−31.6	1655.5	−1.9	1649.6	−7.8	1634.3 [167] <sup>[c]</sup>	−23.1
	1216.9	1196.8	−20.1	1216.8	−0.1	1210.7	−6.2	1189.6 [53] <sup>[c]</sup>	−27.3
NBNCO (D)	2446.7	2429.3	−17.4	2384.4	−62.3	2432.2	−14.5	2445.7 [2266] <sup>[c]</sup>	−1.0
$\text{B}(\text{NCO})_2$ (E)	2341.2	2329.5	−11.7	2276.7	−64.5	2324.0	−17.2	2341.2 [4563] <sup>[c]</sup>	0.0

[a] The frequency shift relative to  $^{10}\text{B}/\text{CO}/\text{N}_2$ . [b] Not observed due to weakness. [c] The IR intensities in square brackets are calculated at the M06-2X-D3/ aug-cc-pVTZ level.

## Theoretical results

### Structures, energies and spectroscopic data

Figure 3 shows the optimized geometries of the five calculated molecules **A–E** in the doublet spin state at the CCSD(T)-Full/cc-pVTZ level of theory and the bond dissociation energies (BDEs) for the loss of two ligands from boron atom. The energetically lowest lying form of the  $\text{BN}_2\text{CO}$  species is the linear molecule **D** ( $C_{\infty v}$ ) which has the connectivity NBNCO. The isomer **A** ( $C_2$ ) with an end-on bonded  $\text{N}_2$  ligand NNBCO is 21.1 kcal mol<sup>-1</sup> higher lying than **D** whereas isomer **B** ( $C_{2v}$ ) with side-on bonded  $\text{N}_2$  ligand  $(\eta^2\text{-N}_2)\text{BCO}$  is 26.2 kcal mol<sup>-1</sup> above the global energy minimum. Molecule **A** is theoretically predicted to have a bending angle of 145.1° at boron. The calculated N–N distance in the side-on bonded isomer **B** is significantly longer (1.253 Å) than in the end-on bond form **A** (1.140 Å), which is only slightly elongated with respect to free  $\text{N}_2$  (1.101 Å). The C–O bonds of the carbonyl ligands in **A** (1.163 Å) and **B** (1.165 Å) are a bit longer than in CO (1.132 Å).

Figure 3 shows that the energetically lowest lying form of the observed  $\text{BN}_2\text{C}_2\text{O}_2$  species is the isomer **E**  $\text{B}(\text{NCO})_2$ , which is 37.7 kcal mol<sup>-1</sup> below structure **C**. The weakly bonded  $\text{N}_2$  in the latter complex **C** has a BDE of only  $D_e = 0.9$  kcal mol<sup>-1</sup>, which is much less than the BDE of dinitrogen in **B**  $(\eta^2\text{-N}_2)\text{BCO}$  ( $D_e = 21.7$  kcal mol<sup>-1</sup>) and in the end-on bonded species **A** NNBCO ( $D_e = 26.9$  kcal mol<sup>-1</sup>). Note that the total BDE of all ligands in **D** (236.3 kcal mol<sup>-1</sup>) and **E** (233.0 kcal mol<sup>-1</sup>) is much higher than in **A** (49.7 kcal mol<sup>-1</sup>), **B** (44.5 kcal mol<sup>-1</sup>) and **C** (83.9 kcal mol<sup>-1</sup>), indicating that the type of binding might be

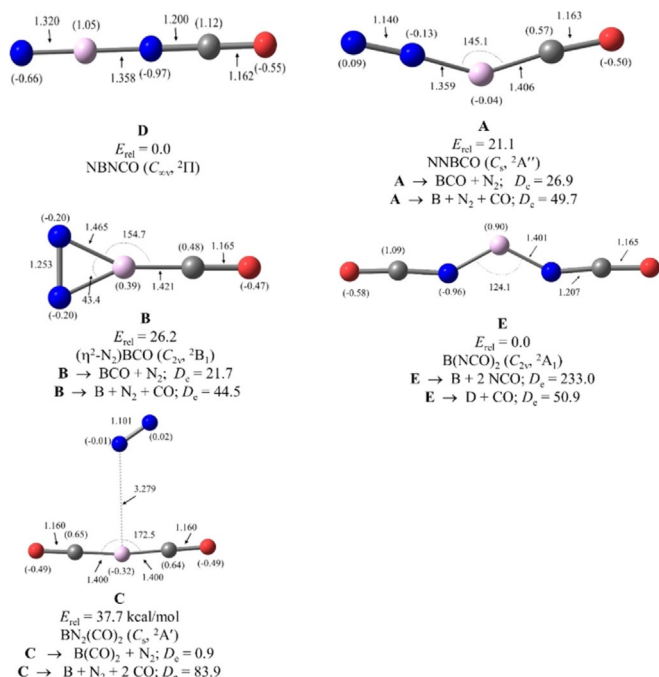


**Figure 3.** The geometries of different isomers of  $\text{BN}_2\text{CO}$  and  $\text{BN}_2(\text{CO})_2$  complexes and bond dissociation energies  $D_e$  at the CCSD(T)-Full/cc-pVTZ level. Bond lengths are in Å and bond angles are in degree. The natural partial charges are given in parentheses. The relative energies and BDEs are given in kcal mol<sup>-1</sup>.

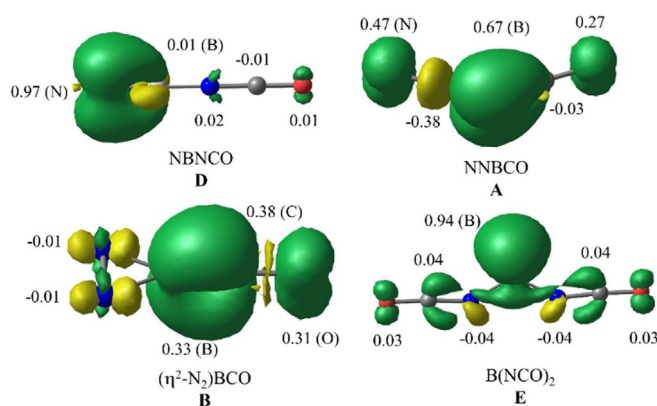
different in the first two molecules than in the last three species.

Table 1 shows the calculated IR frequencies and frequency shifts at the CCSD(T)/cc-pVTZ level of the four isomers **A**, **B**, **D** and **E** in addition to the experimental values. The complete set of vibrational frequencies of all species is given in Table S1 of Supporting Information. The calculated harmonic frequencies are always a bit higher than the experimental values, which come from anharmonic vibrations. Since the vibrational modes come from chemical bonds with very different bond orders and polarities, we did not employ a uniform scaling factor for the computed frequencies. The most important information supporting the assignments of the vibrational spectra come from the frequency shifts of the isotopes with <sup>15</sup>N, <sup>18</sup>O and <sup>11</sup>B atoms in the isomers. There is a very good agreement between the theoretical and experimental isotope shifts, which suggest that the observed IR spectra are correctly assigned to the isomers **A**, **B**, **D** and **E**. IR intensities at CCSD(T)/cc-pVTZ are not available. We calculated the IR spectra at the M06-2X-D3/aug-cc-pVTZ level, which provides also the IR intensities. The results in Table 1 indicate that the calculated vibrational modes of **A**, **B**, **D** and **E** exhibit large IR intensities.

It is interesting to compare the relative isomers of the  $\text{BN}_2\text{CO}$  isomers **A**, **B**, **D** with the analogous beryllium species  $\text{BeN}_2\text{CO}$ , which were recently reported by us.<sup>[31]</sup> The linear isomer NENCO ( $E = \text{Be}$ ,  $B$ ) is in both systems the global energy minimum, but the isomers  $(\eta^2\text{-N}_2)\text{BeCO}$  ( $E_{\text{rel}} = 4.7$  kcal mol<sup>-1</sup>) and NNBeCO ( $E_{\text{rel}} = 5.4$  kcal mol<sup>-1</sup>) are not much higher in energy. The latter species NNBeCO also has a linear structure whereas NNBCO has a bent equilibrium geometry.

### Bonding analysis

We analyzed the electronic structure of the molecules with a variety of theoretical methods. Figure 4 displays the spin density of the various isomers, which indicates the location of the unpaired electron. The unpaired electron of the end-on bonded species **A** NNBCO is delocalized mainly on the NNB fragments and the terminal oxygen atom while in the side-on



**Figure 4.** The spin density plot of different isomers of  $\text{BN}_2\text{CO}$  complex and  $\text{B}(\text{NCO})_2$ . The corresponding values at the CCSD(T)-Full/cc-pVTZ level are given in a.u.



bonded isomer **B** ( $\eta^2$ -N<sub>2</sub>)BCO it is distributed over the BCO moiety. In both cases the unpaired electron occupies a  $\pi$  orbital. In contrast to the delocalized situation in **A** and **B**, the electron in the global energy minimum structure **D** NBNCO is localized at the terminal nitrogen atom, whereas in **E** B(NCO)<sub>2</sub> it is localized at the boron atom.

Important information about the bonding situation in the molecules comes from the atomic charge distribution, which is also shown in Figure 3. The least electronegative boron atom carries, as expected, large positive charges in **D** (1.05 e) and **E** (0.90 e). The positive charge at boron is much smaller in **B** (0.39 e) and it carries even a small negative charge in **A** (−0.04 e). Such an unusual charge distribution was previously reported for molecules where a boron atom binds as a Lewis acid to donor ligands, such as cAAC (cyclic Alkyl Amino Carbene)<sup>[36]</sup> or CO.<sup>[37]</sup> The charge distribution and the calculated BDE values suggest that **A** and **B** may be considered as donor–acceptor complexes of boron with the ligands CO and end-on or side-on bonded N<sub>2</sub>.

We investigated the nature of the interactions between boron and the CO and N<sub>2</sub> ligands in **A** and **B** with the energy decomposition analysis (EDA) in conjunction with natural orbitals for chemical valence (NOCV), which was previously used for related complexes of boron and beryllium.<sup>[11b,c,20,31,32]</sup> Table 2 shows the numerical results of the EDA–NOCV calculations using boron atom with the excited electron configuration  $2s^0 2p_x^2 2p_z^1$ , where  $z$  denotes the out-of-plane coordinate of **A** and **B**, and the ligands [(NN...CO)] as interacting fragments. Calculations using boron atom with the ground state configuration  $2s^2 2p_z^1$  give much larger values for the change in the orbital interactions, which indicates that the former Scheme provides a faithful description of the bonding interaction (see Table S2).<sup>[32,38–40]</sup>

The data in Table 2 show that the attractive boron–ligand interactions in both complexes come mainly from orbital (covalent) bonding, which contribute three quarter of the attraction and that the Coulomb attraction provides one quarter of the binding forces. There are five orbital pairs  $\Delta E_{\text{orb}(1)} - \Delta E_{\text{orb}(5)}$  in **A** and **B**, which can be identified with specific  $\sigma$  or  $\pi$  dative inter-

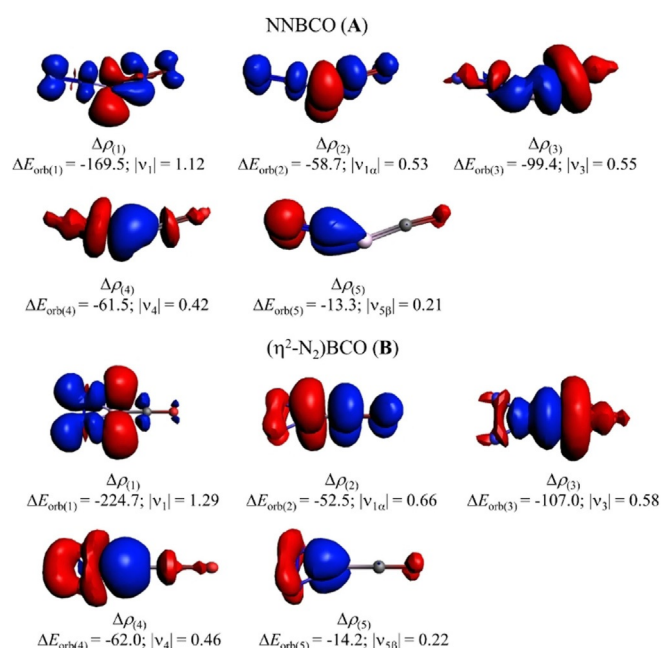


**Figure 5.** Shape of the deformation densities  $\Delta\rho_{(1-5)}$  of NNBCO (**A**) and ( $\eta^2$ -N<sub>2</sub>)BCO (**B**) complexes corresponding to  $\Delta E_{\text{orb}(1-5)}$  at the M06-2X/TZ2P level. Isosurface values are 0.021 a.u. The eigenvalues  $|v_n|$  give the size of the charge migration in e. The direction of the charge flow is red→blue.

actions with the help of the associated deformation densities  $\Delta\rho_{(1)} - \Delta\rho_{(5)}$  shown in Figure 5.

The strongest orbital stabilization  $\Delta E_{\text{orb}(1)}$  comes for both molecules from the in-plane  $\pi_{||}$ -backdonation of the occupied  $2p_{||}$  AO of boron into the in-plane  $\pi^*$  MOs of CO and N<sub>2</sub>. The out-of-plane  $\pi_{\perp}$ -backdonation  $\Delta E_{\text{orb}(2)}$  of the singly occupied  $2p_{\perp}$  AO of boron into the out-of-plane  $\pi^*$  MOs of CO and N<sub>2</sub> is much weaker. There are three components for the donation of the occupied ligands MOs to boron. The strongest contribution  $\Delta E_{\text{orb}(3)}$  comes from the  $\sigma$ -donation of the  $+,-$  combination of the ligand lone-pair MOs into the vacant  $2p_{\sigma}$  AO of boron, followed by the  $\sigma$ -donation  $\Delta E_{\text{orb}(4)}$  of the  $+,+$  combination of the lone-pair MOs into the vacant  $2s$  AO of boron. The weakest

**Table 2.** EDA–NOCV results of the complexes NNBCO (**A**) and ( $\eta^2$ -N<sub>2</sub>)BCO (**B**) at the M06-2X/TZ2P//CCSD(T)-Full/cc-pVTZ level using boron atom in the excited doublet state with the electron configuration ( $2s^2 2p^3$ ) and the NN...CO ligands in the singlet state as interacting fragments. Energy values are in kcal mol<sup>−1</sup>.

Orbital interaction	NNBCO ( <b>A</b> )	( $\eta^2$ -N <sub>2</sub> )BCO ( <b>B</b> )
Fragments	[B] ( $2s^0 2p_{  }^2 2p_{\perp}^1$ ) + [(NN...CO)]	[B] ( $2s^0 2p_{  }^2 2p_{\perp}^1$ ) + [(NN...CO)]
$\Delta E_{\text{int}}$	−353.2	−382.6
$\Delta E_{\text{Pauli}}$	201.1	247.3
$\Delta E_{\text{Metahybrid}}$	23.9	3.1
$\Delta E_{\text{elstat}}^{[a]}$	−153.9 (26.6%)	−143.1 (22.6%)
$\Delta E_{\text{orb}}^{[a]}$	−424.2 (73.4%)	−489.9 (77.4%)
$\Delta E_{\text{orb}(1)}^{[b]}$	[B] ( $2p_{  }^2$ ) → [(NN...CO)] $\pi_{  }$ -backdonation	−169.5 (40.0%)
$\Delta E_{\text{orb}(2)}^{[b]}$	[B] ( $2p_{\perp}^1$ ) → [(NN...CO)] $\pi_{\perp}$ -backdonation	−58.7 (13.8%)
$\Delta E_{\text{orb}(3)}^{[b]}$	[B] ( $2p_{\sigma}^0$ ) ← [(NN...CO)] $(+,-)$ $\sigma$ -donation	−99.4 (23.4%)
$\Delta E_{\text{orb}(4)}^{[b]}$	[B] ( $2s^0$ ) ← [(NN...CO)] $(+,+)$ $\sigma$ -donation	−61.5 (14.5%)
$\Delta E_{\text{orb}(5)}^{[b]}$	[B] ( $2p_{\perp}^1$ ) ← [(NN...CO)] $\pi_{\perp}$ -donation	−13.3 (3.1%)
$\Delta E_{\text{orb}(\text{rest})}^{[b]}$		−21.8 (5.1%)
		−29.5 (6.0%)

[a] The values within the parentheses show the contribution towards the total attractive interaction  $\Delta E_{\text{elstat}} + \Delta E_{\text{orb}}$ . [b] The values within the parentheses show the contribution towards the total orbital interaction,  $\Delta E_{\text{orb}}$ .

orbital contribution  $\Delta E_{\text{orb}(5)}$  is due to the  $\pi_{\perp}$ -donation of the occupied  $\pi_{\perp}$  MOs of the ligands into the singly occupied  $2p_{\perp}$  AO of boron. It is gratifying that the EDA-NOCV method provides not only numerical results of the orbital interactions but also visualizes the associated changes in the electronic structures with the help of the deformation densities.

### Reaction mechanism

The calculated reaction mechanism, which is suggested for the formation of the experimentally observed molecules **B**, **D** and **E** starting from **A** is outlined in Figure 6. The energy minima and transition states were optimized at the M06-2X-D3/aug-cc-pVTZ level with subsequent energy calculations at CCSD(T)-Full/cc-pVTZ. The energy differences between the minimum structures **A**, **B**, **D** and **E** are therefore slightly different from the values in Figure 3. The experimental observations clearly show that the ground state boron atoms react with carbon monoxide and dinitrogen to form the end-on bonded NNBCO (**A**) complex on annealing in both neon and dinitrogen matrices. This addition reaction is exothermic and requires no activation energy. The absorptions of complex **B** are produced under visible light (435–480 nm) irradiation when the NNBCO (**A**) absorptions decrease, indicating that the end-on bonded NNBCO (**A**) complex isomerizes to complex **B** with a side-on bonded  $\text{N}_2$  ligand. This isomerization reaction is predicted to be slightly endothermic by  $5.0 \text{ kcal mol}^{-1}$  and proceeds via a transition state **TS-1** lying  $51.1 \text{ kcal mol}^{-1}$  above complex **A** at the CCSD(T)-Full/cc-pVTZ//M06-2X-D3/aug-cc-pVTZ level. The reaction involves the change of the  $\sigma$  bonded  $\text{N}_2$  species **A** to the  $\pi$  bonded  $\text{N}_2$  isomer **B** where the loss of strong  $\sigma$  interaction in **TS-1** leads to a large barrier.

The complex **B** absorptions were destroyed under UV light irradiation with the production of species **D** and **E**, in which the N–N bond is completely cleaved. The isomerization reaction from **B** to **D** is exothermic by  $26.5 \text{ kcal mol}^{-1}$  and proceeds via an energetically high lying four-membered ring intermediate **I**, which is formed with a barrier **TS-2** of  $45.1 \text{ kcal mol}^{-1}$  relative to **B**. The ring-opening reaction **I**→**D** proceeds with an even higher-lying transition state **TS-3**, which is  $32.7 \text{ kcal mol}^{-1}$

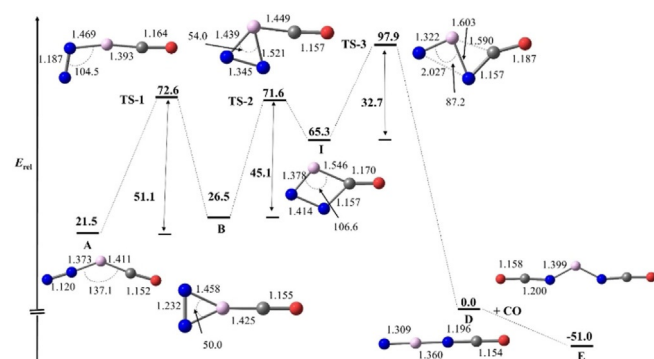


**Figure 6.** The computed **A**→**D**→**E** isomeric transformation pathway at the M06-2X-D3/aug-cc-pVTZ level. The relative energies are in  $\text{kcal mol}^{-1}$  at the CCSD(T)-Full/cc-pVTZ//M06-2X-D3/aug-cc-pVTZ level. Bond distances are in Å and angles are in degree.

above **I** and  $71.4 \text{ kcal mol}^{-1}$  above **B**. The very large barrier may be the reason for the low yield of the energetically lowest lying isomer **D**. Species **E** may then be formed via CO addition to **D**, which is exothermic by  $51.0 \text{ kcal mol}^{-1}$ . These isomerization reactions are photon-induced processes, in which some excited states may be involved. The predicted barriers are in reasonable agreement with the experimental observation that complex **A** isomerizes to complex **B** under visible light irradiation, while complex **B** rearranges to isomer **D** under UV light excitation.

### Conclusions

The experimental results of this work show that boron atoms react with carbon monoxide and dinitrogen in forming the end-on bonded NNBCO complex in solid neon or nitrogen matrices. The NNBCO complex rearranges to the  $(\eta^2\text{-N}_2)\text{BCO}$  isomer with a more activated side-on bonded dinitrogen ligand upon visible light excitation.  $(\eta^2\text{-N}_2)\text{BCO}$  and its weakly CO-coordinated complexes further isomerize to the NBNCO and  $\text{B}(\text{NCO})_2$  molecules with N–N bond being completely cleaved under UV light irradiation. The quantum chemical calculations show that the energetically lowest lying  $\text{BN}_2\text{CO}$  isomer is the isocyanate species NBNCO, which is  $21.1 \text{ kcal mol}^{-1}$  more stable than the end-on bonded NNBCO complex and  $26.2 \text{ kcal mol}^{-1}$  lower in energy than the side-on bonded  $(\eta^2\text{-N}_2)\text{BCO}$  isomer.

### Acknowledgements

The experimental work was supported by the National Natural Science Foundation of China (grant number 21688102). L.Z. and G.F. acknowledge financial support from Nanjing Tech University (grant numbers 39837123, 39837132) and SICAM Fellowship from Jiangsu National Synergetic Innovation Center for Advanced Materials, Natural Science Foundation of Jiangsu Province for Youth (grant number BK20170964), National Natural Science Foundation of China (grant number 21703099). S.P. thanks Nanjing Tech University for a postdoctoral fellowship and the high performance center of Nanjing Tech University for the computational resources. S.P. and G.F. acknowledges financial support by the Deutsche Forschungsgemeinschaft. Open access funding enabled and organized by Projekt DEAL.

### Conflict of interest

The authors declare no conflict of interest.

**Keywords:** bonding analysis • boron • IR spectroscopy • matrix isolation •  $\text{N}_2$  fixation and activation

- [1] D. E. Canfield, A. N. Glazer, P. G. Falkowski, *Science* **2010**, *330*, 192–196.
- [2] B. M. Hoffman, D. Lukoyanov, Z. Y. Yang, D. R. Dean, L. C. Seefeldt, *Chem. Rev.* **2014**, *114*, 4041–4062.

- [3] R. Schlögl, *Ammonia Synthesis in Handbook of Homogeneous Catalysis* (Eds.: G. Ertl, H. Knözinger, F. Schüth, J. Weitkamp), chapter 12.1, pp. 2501–2574, Wiley, 2008.
- [4] a) M. Hiday, Y. Mizobe, *Chem. Rev.* **1995**, *95*, 1115–1133; b) B. A. Mackay, M. D. Fryzuk, *Chem. Rev.* **2004**, *104*, 385–402; c) R. J. Burford, A. Yeo, M. D. Fryzuk, *Coord. Chem. Rev.* **2017**, *334*, 84–99.
- [5] a) D. V. Yandulov, P. R. Schrock, *Science* **2003**, *301*, 76–78; b) N. Hazari, *Chem. Soc. Rev.* **2010**, *39*, 4044–4056; c) K. C. MacLeod, P. L. Holland, *Nat. Chem.* **2013**, *5*, 559–565; d) H. Tanaka, Y. Nishibayashi, K. Yoshizawa, *Acc. Chem. Res.* **2016**, *49*, 987–995; e) C. Geng, J. Li, T. Weiske, H. Schwarz, *Proc. Natl. Acad. Sci. USA* **2018**, *115*, 11680–11687; f) C. Geng, J. Li, T. Weiske, H. Schwarz, *Proc. Natl. Acad. Sci. USA* **2019**, *116*, 21416–21420.
- [6] H. J. Himmel, M. Reiher, *Angew. Chem. Int. Ed.* **2006**, *45*, 6264–6288; *Angew. Chem.* **2006**, *118*, 6412–6437.
- [7] M. Falcone, L. Chatelain, R. Scopelliti, I. Zivkovic, M. Mazzanti, *Nature* **2017**, *547*, 332–335.
- [8] a) M. A. Légaré, G. Bélanger-Chabot, R. D. Dewhurst, E. Welz, I. Krumm-nacher, B. Engels, H. Braunschweig, *Science* **2018**, *359*, 896–900; b) D. L. Broere, P. L. Holland, *Science* **2018**, *359*, 871.
- [9] a) C. Hering-Junghans, *Angew. Chem. Int. Ed.* **2018**, *57*, 6738–6740; *Angew. Chem.* **2018**, *130*, 6850–6852; b) C. Ling, X. Niu, Q. Li, A. Du, J. Wang, *J. Am. Chem. Soc.* **2018**, *140*, 14161–14168; c) C. W. Liu, Q. Y. Li, C. Z. Wu, J. Zhang, Y. G. Jin, D. R. MacFarlane, C. H. Sun, *J. Am. Chem. Soc.* **2019**, *141*, 2884–2888.
- [10] M. A. Légaré, M. Rang, G. Bélanger-Chabot, J. I. Schweizer, I. Krumm-nacher, R. Bertermann, M. Arrowsmith, M. C. Holthausen, H. Braunschweig, *Science* **2019**, *363*, 1329–1332.
- [11] a) C. A. Thompson, L. Andrews, R. D. Davy, *J. Phys. Chem.* **1995**, *99*, 7913–7924; b) G. H. Deng, S. Pan, G. J. Wang, L. L. Zhao, M. F. Zhou, G. Frenking, *Angew. Chem. Int. Ed.* **2020**, *59*, 10603–10609; *Angew. Chem.* **2020**, *132*, 10690–10696; c) Q. Wang, S. Pan, S. J. Lei, J. Y. Jin, G. H. Deng, G. J. Wang, L. L. Zhao, M. F. Zhou, G. Frenking, *Nat. Commun.* **2019**, *10*, 3375.
- [12] a) G. Maier, H. P. Reisenauer, J. Henkelmann, C. Kliche, *Angew. Chem. Int. Ed. Engl.* **1988**, *27*, 295–296; *Angew. Chem.* **1988**, *100*, 303–303; b) K. Edel, M. Krieg, D. Grote, H. F. Bettinger, *J. Am. Chem. Soc.* **2017**, *139*, 15151–15159.
- [13] H. J. Himmel, N. Hebben, *Chem. Eur. J.* **2005**, *11*, 4096–4102.
- [14] a) R. R. Lembke, R. F. Ferrante, W. Weltner, Jr., *J. Am. Chem. Soc.* **1977**, *99*, 416–423; b) M. Winkler, W. Sander, *J. Org. Chem.* **2006**, *71*, 6357–6367.
- [15] D. Kurzbach, A. Sharma, D. Sebastiani, K. W. Klinkhammer, D. Hinderberger, *Chem. Sci.* **2011**, *2*, 473–479.
- [16] J. Y. Jin, G. J. Wang, M. F. Zhou, D. M. Andrada, M. Hermann, G. Frenking, *Angew. Chem. Int. Ed.* **2016**, *55*, 2078–2082; *Angew. Chem.* **2016**, *128*, 2118–2122.
- [17] a) D. L. Robbins, L. R. Brock, J. S. Pilgrim, M. A. Duncan, *J. Chem. Phys.* **1995**, *102*, 1481–1492; b) S. H. Pullins, J. E. Reddic, M. R. France, M. A. Duncan, *J. Chem. Phys.* **1998**, *108*, 2725–2732; c) L. R. Brock, M. A. Duncan, *J. Phys. Chem.* **1995**, *99*, 16571–16575.
- [18] a) D. J. Knobloch, E. Lobkovsky, P. J. Chirik, *J. Am. Chem. Soc.* **2010**, *132*, 10553–10564; b) D. J. Knobloch, S. P. Sempronii, E. Lobkovsky, P. J. Chirik, *J. Am. Chem. Soc.* **2012**, *134*, 3377–3386.
- [19] X. H. Zhang, B. Butschke, H. Schwarz, *Chem. Eur. J.* **2010**, *16*, 12564–12569.
- [20] Z. J. Lv, Z. Huang, W. X. Zhang, Z. F. Xi, *J. Am. Chem. Soc.* **2019**, *141*, 8773–8777.
- [21] Z. H. Lu, Q. Xu, *Phys. Chem. Chem. Phys.* **2010**, *12*, 7077–7082.
- [22] H. J. Himmel, A. J. Downs, T. M. Greene, *Chem. Rev.* **2002**, *102*, 4191–4241.
- [23] a) L. Andrews, T. J. Tague, G. P. Kushto, *Inorg. Chem.* **1995**, *34*, 2952–2961; b) W. L. Li, Q. N. Zhang, M. H. Chen, H. S. Hu, J. Li, M. F. Zhou, *Angew. Chem. Int. Ed.* **2020**, *59*, 6923–6928; *Angew. Chem.* **2020**, *132*, 6990–6995.
- [24] X. Wu, L. L. Zhao, J. Y. Jin, S. Pan, W. Li, X. Y. Jin, G. J. Wang, M. F. Zhou, G. Frenking, *Science* **2018**, *361*, 912–916.
- [25] a) Y. M. Hamrick, R. J. V. Zee, J. T. Godbout, W. Weltner, W. J. Lauderdale, J. F. Stanton, R. J. Bartlett, *J. Phys. Chem.* **1991**, *95*, 2840–2844; b) T. R. Burkholder, L. Andrews, *J. Phys. Chem.* **1992**, *96*, 10195–10201; c) M. F. Zhou, N. Tsumori, L. Andrews, Q. Xu, *J. Phys. Chem. A* **2003**, *107*, 2458–2463.
- [26] a) M. F. Zhou, Z. X. Wang, P. R. Schleyer, Q. Xu, *ChemPhysChem* **2003**, *4*, 763–766; b) M. F. Zhou, N. Tsumori, Z. H. Li, K. N. Fan, L. Andrews, Q. Xu, *J. Am. Chem. Soc.* **2002**, *124*, 12936–12937; c) M. F. Zhou, Q. Xu, Z. X. Wang, P. R. Schleyer, *J. Am. Chem. Soc.* **2002**, *124*, 14854–14855.
- [27] a) J. W. Jian, J. Y. Jin, H. Qu, H. L. Lin, M. H. Chen, G. J. Wang, M. F. Zhou, D. M. Andrada, M. Hermann, G. Frenking, *Chem. Eur. J.* **2016**, *22*, 2376–2385; b) J. Y. Jin, M. F. Zhou, *Dalton Trans.* **2018**, *47*, 17192–17197.
- [28] a) P. H. Kasai, P. M. Jones, *J. Am. Chem. Soc.* **1984**, *106*, 8018–8020; b) J. H. B. Chenier, C. A. Hampson, J. A. Howard, B. Mile, R. Sutcliffe, *J. Phys. Chem.* **1986**, *90*, 1524–1528; c) C. Xu, L. Manceron, J. P. Perchard, *J. Chem. Soc. Faraday Trans.* **1993**, *89*, 1291–1298; d) H. J. Himmel, A. J. Downs, J. C. Greene, T. M. Greene, *J. Phys. Chem. A* **2000**, *104*, 3642–3654; e) W. G. Hatton, N. P. Hacker, P. H. Kasai, *J. Phys. Chem.* **1989**, *93*, 1328–1332.
- [29] a) M. F. Zhou, L. Jiang, Q. Xu, *J. Chem. Phys.* **2004**, *121*, 10474–10482; b) A. Feltrin, S. N. Cesaro, F. Ramondo, *Vib. Spectrosc.* **1996**, *10*, 139–146; c) M. F. Zhou, L. Jiang, Q. Xu, *J. Phys. Chem. A* **2005**, *109*, 3325–3330; d) A. Bos, *J. Chem. Soc. Chem. Commun.* **1972**, 26b–27; e) L. Jiang, Q. Xu, *J. Chem. Phys.* **2005**, *122*, 034505.
- [30] a) L. N. Zhang, J. Dong, M. F. Zhou, *Chem. Phys. Lett.* **2001**, *335*, 334–338; b) A. J. Bridgeman, N. Harris, N. A. Young, *Chem. Commun.* **2000**, 1241–1242.
- [31] G. H. Deng, S. Pan, G. J. Wang, L. L. Zhao, M. F. Zhou, G. Frenking, *Angew. Chem. Int. Ed.* **2020**, *59*, 18201–18207.
- [32] Q. N. Zhang, W. L. Li, C. Q. Xu, M. H. Chen, M. F. Zhou, J. Li, D. M. Andrada, G. Frenking, *Angew. Chem. Int. Ed.* **2015**, *54*, 11078–11083; *Angew. Chem.* **2015**, *127*, 11230–11235.
- [33] a) P. Hassanzadeh, L. Andrews, *J. Phys. Chem.* **1992**, *96*, 9177–9182; b) L. Andrews, P. Hassanzadeh, T. R. Burkholder, *J. Chem. Phys.* **1993**, *98*, 922–931.
- [34] M. H. Chen, Q. Y. Kong, M. F. Zhou, *J. Mol. Struct.* **2003**, *657*, 101–105.
- [35] a) H. Mongeot, H. R. Atchekzai, M. Fouassier, M. T. Forel, *J. Mol. Struct.* **1980**, *62*, 35–46; b) H. Goubeau, H. Gräbner, *Chem. Ber.* **1960**, *93*, 1379–1387; c) M. Alaei, E. G. Livingstone, N. P. C. Westwood, *J. Am. Chem. Soc.* **1993**, *115*, 2871–2876.
- [36] R. Kinjo, B. Donnadiu, M. A. Celik, G. Frenking, G. Bertrand, *Science* **2011**, *333*, 610–613.
- [37] H. Braunschweig, R. D. Dewhurst, F. Hupp, M. Nutz, K. Radacki, C. W. Tate, A. Vargas, Q. Ye, *Nature* **2015**, *522*, 327–330.
- [38] a) D. M. Andrada, G. Frenking, *Angew. Chem. Int. Ed.* **2015**, *54*, 12319–12324; *Angew. Chem.* **2015**, *127*, 12494–12500; b) C. Mohapatra, S. Kundu, A. N. Paesch, R. Herbst-Irmer, D. Stalke, D. M. Andrada, G. Frenking, H. W. Roesky, *J. Am. Chem. Soc.* **2016**, *138*, 10429–10432; c) L. T. Scharf, M. Andrada, G. Frenking, *Chem. Eur. J.* **2017**, *23*, 4422–4434; d) M. Hermann, G. Frenking, *Chem. Eur. J.* **2017**, *23*, 3347–3356.
- [39] a) D. C. Georgiou, L. Zhao, D. J. D. Wilson, G. Frenking, J. L. Dutton, *Chem. Eur. J.* **2017**, *23*, 2926–2934; b) D. M. Andrada, J. L. Casal-Sainz, A. M. Pendas, G. Frenking, *Chem. Eur. J.* **2018**, *24*, 9083–9089; c) R. Saha, S. Pan, G. Merino, P. K. Chattaraj, *Angew. Chem. Int. Ed.* **2019**, *58*, 8372–8377; *Angew. Chem.* **2019**, *131*, 8460–8465.
- [40] Q. Wang, S. Pan, Y. Wu, G. Deng, G. Wang, L. Zhao, M. Zhou, G. Frenking, *Angew. Chem. Int. Ed.* **2019**, *58*, 17365–17374; *Angew. Chem.* **2019**, *131*, 17526–17535.

Manuscript received: September 27, 2020

Accepted manuscript online: September 29, 2020

Version of record online: December 21, 2020